ACS OMEGA

http://pubs.acs.org/journal/acsodf

Article

Study of Electrochemical Catalytic Coal Gasification: Gasification Characteristics and Char Structure Evolution

Fan Yang, Qingbo Yu,* Wenjun Duan, Zhenfei Qi, and Qin Qin

Cite This: *ACS Omega* 2021, 6, 31026−31036

Read Online

ACCESS | Metrics & More | Article Recommendations

ABSTRACT: Electrochemical catalytic coal gasification experiments with Fuxin (FX) coal under a CO_2 atmosphere were conducted to evaluate the effects of power and temperature on coal gasification and char structure evolution during electrochemical catalytic gasification (ECG). When the power was 400 W, with temperature increasing from 800 to 1000 °C, the CO content in the gas products increased by 8.16%, the H_2 content increased by 8.39%, and the CH_4 concentration in the gas products initially increased and then decreased. When the temperature is 900 °C, with power increasing from 0 to 400 W, the CO content in the gas products increased by 58.27%, the H_2 content increased by 81.33%, and the CH_4 concentration in the gas products increased from 1.31 to 2.37%. The gasification reactivity and the concentration of combustible gas generated during ECG were higher than those during common coal gasification. Thermal electrons play important roles in ECG. These electrons could promote ring opening reactions and aromatic compound cracking and inhibit aromatization reactions while increasing the number of oxygen-containing functional groups in char, consequently enhancing the char gasification reactivity.

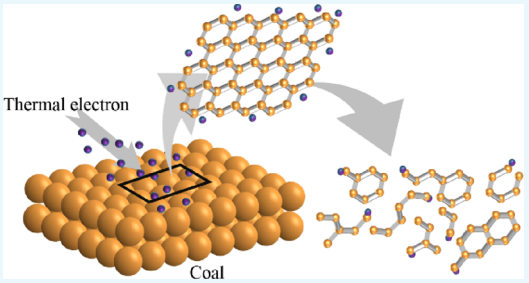

1. INTRODUCTION

The energy demand in China is continuously increasing because of its rapidly developing economy. According to the Statistical Review of World Energy 2020,[1] coal consumption by China accounted for 58.24% of the global energy consumption recorded for 2018. Coal is still the primary energy resource for China. Therefore, to adhere to international requirements for energy conservation and emission reduction, efficient coal conversion and the development of clean and green processes based on coal are still essential.

Coal gasification is an important method for implementing clean coal utilization;[2] however, its efficiency requires improvement. As an effective method for improving the efficiency, catalytic gasification is a promising topic that could decrease the thermochemical reaction temperature, enhance the carbon conversion rate, reduce the investment cost, and selectively create syngas needed for the production of downstream products by altering the reaction pathway.[3−5] Research on catalytic gasification primarily focuses on catalyst development; the most commonly employed catalysts include single catalysts containing alkali or alkali earth metals, composite catalysts, and disposable catalysts (e.g., natural ore and industrial waste). Catalysts with lithium and potassium alkali metals are the most effective among the simple catalysts because they efficiently promote coal gasification.[6,7] However, potassium and sodium evaporate during high-temperature gasification, making it difficult to maintain catalytic performance. Alkaline earth metals such as calcium or group VIII metals are commonly utilized,[8−10] and their performance can be maintained in gasified char. However, their catalytic activity is considerably lower than the activity of catalysts with alkali metals.[8,11] Obviously, single catalysts cannot meet the catalytic demands of the gasification process (i.e., high reactivity, stability toward deactivation, and selectivity) due to the complexity of the process. According to current studies, composite catalysts are superior to single-component catalysts in numerous characteristics.[12−14] Furthermore, disposable catalysts such as inexpensive and readily available ore (e.g., limestone,[15] dolomite,[16] low-grade iron ore,[17] and limonite[18]) as well as alkali liquor, alkali residue, and black liquor industrial waste[19−22] could promote gasification. However, the industrial-scale development of all these catalysts is challenging because of high operating and recovery costs, extensive equipment corrosion, and secondary pollution to the environment. Disposable catalysts have lower efficiency than conventional composite catalysts. Thus, it is essential to design novel, cost-effective catalyst gasification methods that improve coal

Received: August 3, 2021
Accepted: November 4, 2021
Published: November 12, 2021

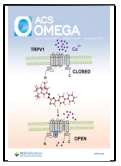

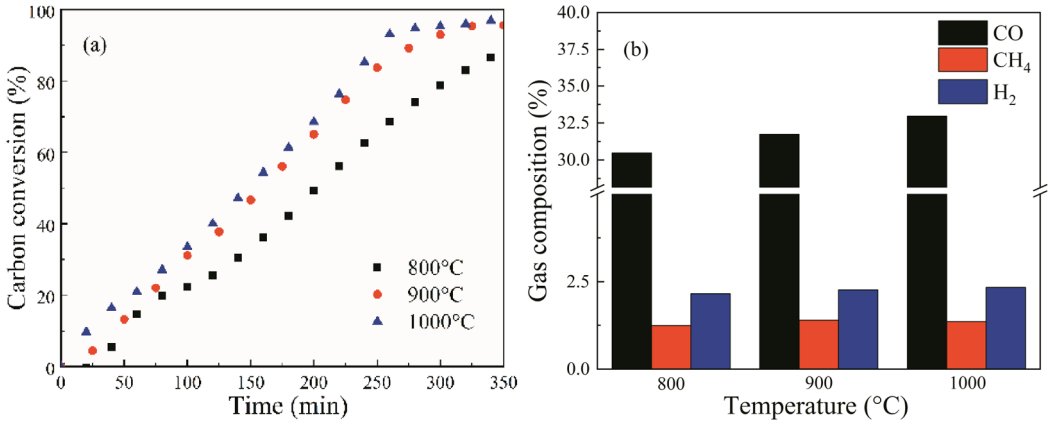

Figure 1. Effects of temperature on (a) carbon conversion and (b) main combustible gas composition.

gasification efficiency by operation at reasonable gasification temperatures.

Electrons will flow through a metal wire when an alternating current is passed through it, and the metal surface is left by some of these electrons to create thermal electrons in the gas phase. This process is known as thermal electron emission.[23,24] Some Ca−Al−O materials can be used to store and emit X^- anions.[25−31] When electricity is applied to these materials, electrons are supplied to the material surface, where they subsequently enter the body of the material. These electrons can replace the anions lost by emission and keep the charge of the material neutral.[29,32] The consumed anions (X^-) could then be regenerated by the molecules reacting with the thermal electrons.[33] Based on these anionic emission material studies, a technique to reform bio-oil with high energy efficiency, electrochemical catalytic reforming, was established. In this technique, using an electrified Ni−Cr wire, the catalyst is heated and simultaneously provided with thermal electrons.[24,32,34−38] Thermal electrons improve the decomposition and reforming of organic compounds in the bio-oil and reduce Ni^{2+} in the catalyst while playing important roles in increasing the carbon conversion rate and hydrogen yield. Relatively large quantities of organic compounds exist in char and coal. By supplying a current to coal, the gasification procedure may be improved by the resulting thermal electrons. Thus, we propose an electrochemical catalytic gasification (ECG) method for coal.[39] This new method is expected to mitigate the problems commonly encountered with conventional catalysts during industrial-scale development.

In prior research, we focused a lot on confirming the feasibility of ECG. However, the effects of temperature and thermal electrons on gas production and the char structure during the ECG process still need further research. It has important guiding significance for the practical application of this new method. Therefore, in this study, the effects of temperature and power on the ECG of coal were studied. The composition of combustible gases (CO, H_2, and CH_4) produced by each process and their carbon conversion rates were estimated. An explanation for ECG was also provided.

2. RESULTS AND DISCUSSION

2.1. Effects of Temperature. ECG carbon conversion was investigated as a function of time at a fixed power of 400 W with varying temperatures (Figure 1a), where the carbon conversion was seen to gradually increase with increasing temperature.

When the power was 400 W, the calculation results of $R_{0.5}$ under different temperature conditions are shown in Figure 2.

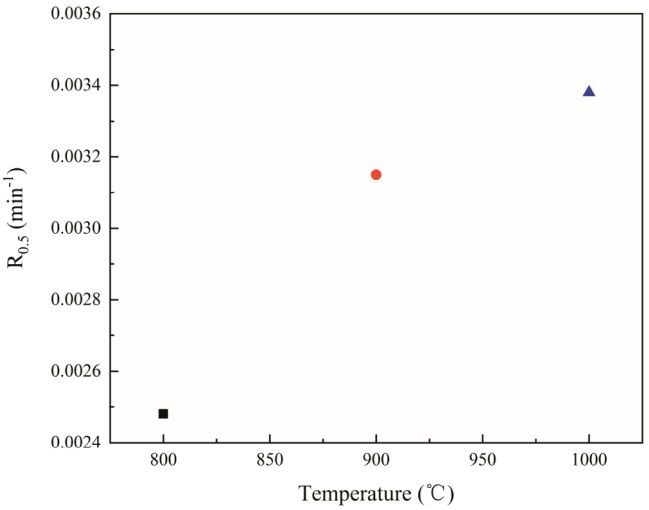

Figure 2. $R_{0.5}$ under different temperature conditions.

The $R_{0.5}$ increased from 0.00248 to 0.00338 min^{-1} with increasing temperature; therefore, we concluded that higher temperatures mean higher efficiency of the coal gasification reaction during ECG because the overall reaction of coal gasification is endothermic. Increasing the temperature is beneficial to the consumption of C in coal, which leads to an increase in carbon conversion at the same reaction time.

The main components of gas production were CO, CO_2, H_2, and CH_4, and their compositions during ECG at different temperatures were analyzed (Figure 1b). As the temperature increased, the CO and H_2 concentrations increased, but the CH_4 concentration only initially increased and then steadily decreased because the overall reaction of coal gasification is endothermic. Increasing the temperature is beneficial to the formation of CO and the consumption of CO_2 and C in coal. As the temperature increases, more organic compounds in the coal decompose to give H_2 and CH_4, and the latter subsequently reacts with CO_2 and H_2O to form CO and more H_2.

2.2. Effect of Power. The ECG carbon conversion was also evaluated as a function of time at a fixed temperature of 900 °C with varying powers: 100, 200, 300, and 400 W (Figure 3a). When the power was 0 W, the coal was gasified in CCG.

https://doi.org/10.1021/acsomega.1c04135
ACS Omega 2021, 6, 31026−31036

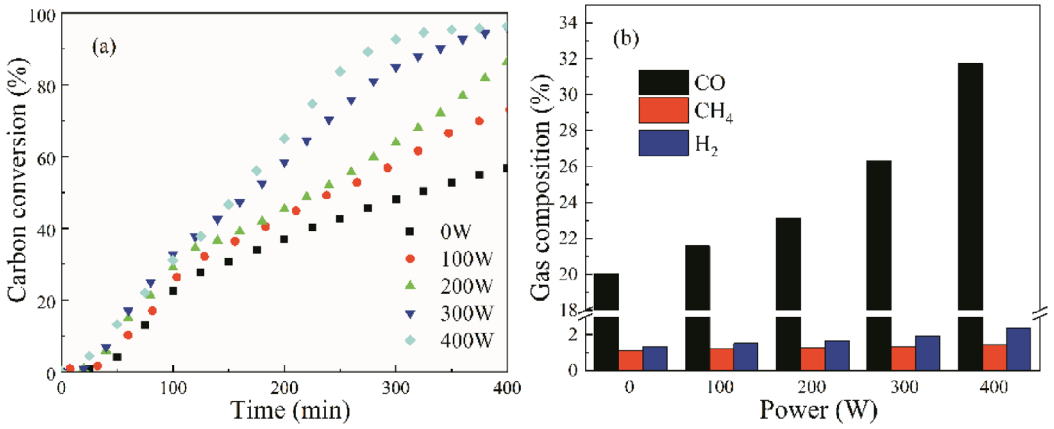

Figure 3. Effects of power on (a) carbon conversion and (b) main combustible gas composition.

As shown in Figure 3a, the carbon conversion of coal during ECG was higher than during CCG. As the power increased, the carbon conversion also gradually increased during ECG.

When the temperature was 900 °C, the calculation results of $R_{0.5}$ under different power conditions are shown in Figure 4.

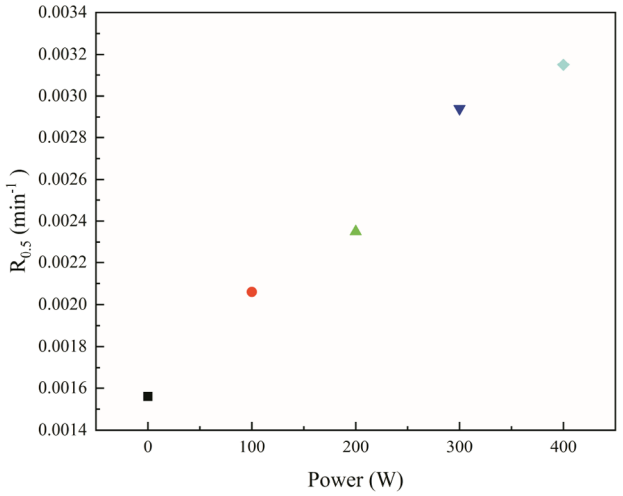

Figure 4. $R_{0.5}$ under different power conditions.

The $R_{0.5}$ increased from 0.00156 to 0.00315 min^{-1} with increasing power, demonstrating that the greater power given to the Ni−Cr wire during this process promotes higher gasification reactivity.

Moreover, the main combustible gas compositions during ECG were determined at different powers (Figure 3b). When the power was 0 W, coal was gasified in CCG. Increasing the power during ECG was found to increase the concentrations of CO, CH_4, and H_2. Overall, the combustible gas concentrations generated during ECG were higher than those produced during CCG.

2.3. Explanation for ECG. Figure 5 represents the degree of carbon conversion under various circumstances in comparative experiments. The conversion of carbon under condition (b) was approximately similar to that under condition (a). It can be seen that the Ni−Cr wire does not seem to have much effect on the improvement of coal gasification reaction during ECG. This requires in-depth analysis in combination with other test results. The conversion of carbon under condition (d) was slightly higher than that

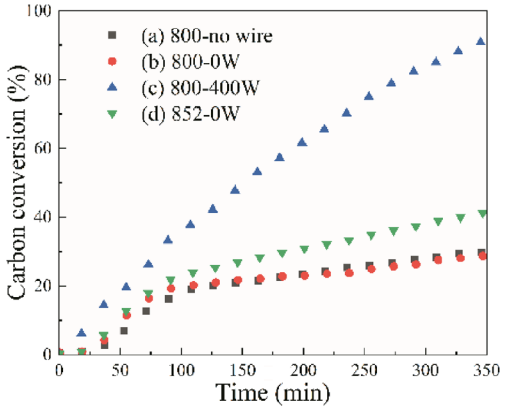

Figure 5. Conversion of carbon under various circumstances in the comparative experiment.

under condition (b). By increasing the coalbed temperature, the coal gasification efficiency was improved. However, the conversion of carbon in ECG (condition c) was greater than that in condition (d). Therefore, local heating did not improve the performance in ECG; however, the performance improved by the existence of thermal electrons, which played a key role in ECG.

The gasification reactivity of coal is associated with its structural features.[40] To confirm this speculation, the crystalline states of the char carbon structure and chemical structures were characterized. The selected char samples at a relative carbon conversion of nearly 50% were prepared during the comparative experiments. The crystalline states of the char carbon structures obtained from the comparative experiments were investigated by XRD. Typical XRD spectra were collected for the char obtained under conditions (a−d) (Figure 7).

The high background intensity shown in Figure 7 indicates that some disordered substances in char are in the form of amorphous carbon.[41] Moreover, peaks clearly representing the (002) and (100) planes at approximately 26 and 43°, respectively, appeared in the diffraction patterns, indicating that the char samples also contained some crystalline carbon. All these observations suggest that turbostratic structures or random layer lattice structures exist in the crystallites of all the coals. In the diffraction profile, the (γ) band appearing at approximately 23° was associated with a saturated structure connected to the edge of the coal crystallite, such as an aliphatic side chain.[42,43] The (002) plane peak reflected the

https://doi.org/10.1021/acsomega.1c04135
ACS Omega 2021, 6, 31026−31036

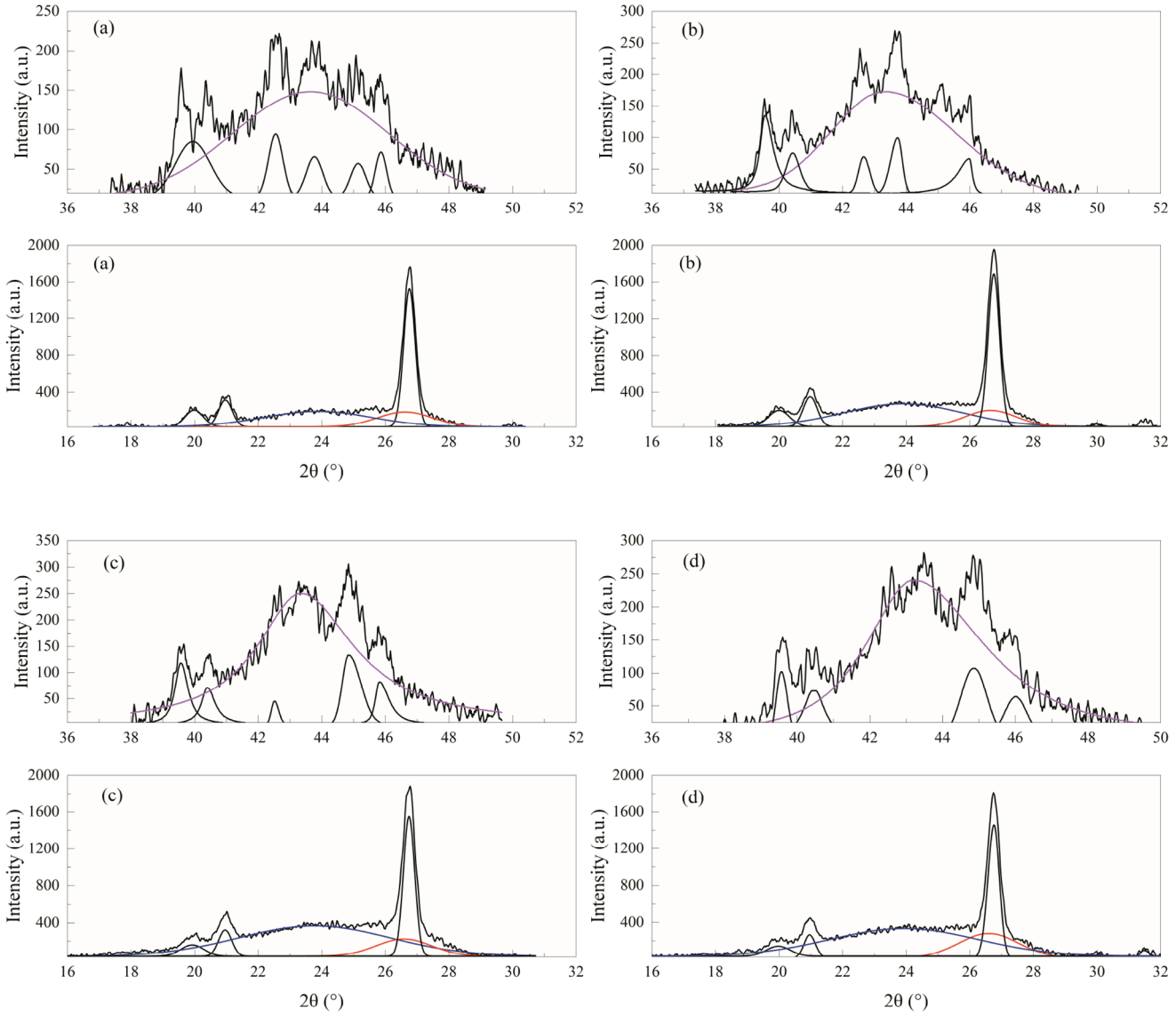

Figure 6. Curve fitting of peaks for coal char obtained under (a–d) conditions in 2θ ranges of 16–32 and 36–52°.

spacing of the aromatic ring layers, and the (γ) band indicated the packing distance of the saturated structures.

Curve fitting was performed on the diffractograms at approximately 23, 26, and 43° using a Gaussian function. The curve fittings of peaks for coal char obtained under (a–d) conditions in 2θ ranges of 16–332 and 36–552° are shown in Figure 6. The derived structural parameters were calculated,[43] and the results are summarized in Table 1.

The L_c of char obtained under condition (b) was decreased compared to that of char obtained under condition (a), and the L_a of char obtained under condition (b) was increased compared to that of char obtained under condition (a). The f_a of char obtained under condition (a) was higher than that of char obtained under condition (b), while the crystallinity of char obtained under condition (b) was higher than that of condition (a). This suggested that adding the Ni–Cr alloy wire induced carbon crystallization, such as graphite, to appear in the char and produced char with a higher degree of ordered carbon. It is because that Ni in the alloy wire can accelerate the condensation of char, which leads to a higher degree of the ordered carbon structure in char.[43,44] The crystallinity of char obtained under condition (d) was higher than that of char provided under condition (b). This result indicates that the char produced by ECG will exhibit more crystalline carbons (e.g., graphite) and a higher degree of ordered carbon at higher coalbed temperatures near the Ni–Cr alloy wire. Increasing the temperature could promote crystallite growth.[41]

The L_c and L_a of char obtained under condition (c) were lower than those of char produced under other conditions, which means that the longitudinal and transverse dimensions of char microcrystalline structural units decreased during ECG. Moreover, the crystallinity and f_a obtained under condition (c) were lower than those achieved under other conditions. This shows that the release of thermal electrons caused the lower crystallinity and higher reactivity of the coal char as well as the decreasing longitudinal and transverse sizes of its microcrystalline structure. To verify this result, the gasification reactivity of coal char samples obtained under different conditions in comparative experiments was measured using TGA (NETZSCH STA 449, Germany). A char sample (8 mg) was placed in an alumina crucible and heated at a 20 °C/min rate in each test. Reactor heating was performed to 1000 °C in

https://doi.org/10.1021/acsomega.1c04135
ACS Omega 2021, 6, 31026–31036

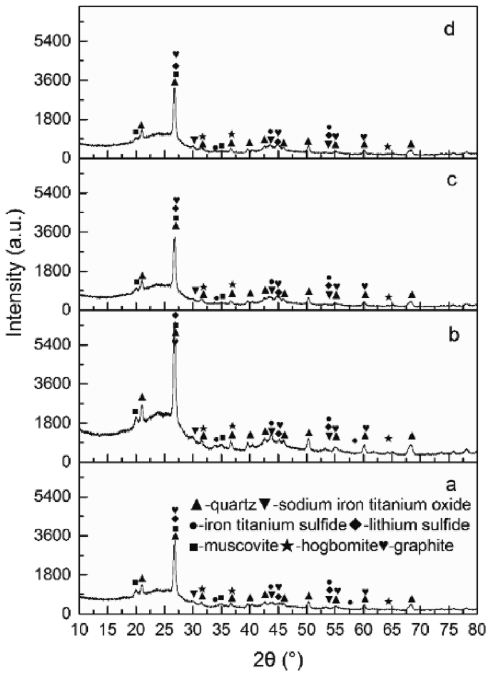

Figure 7. XRD spectra for the char obtained under different conditions in a comparative experiment: (a) 800 °C, no wire; (b) 800 °C, 0 W; (c) 800 °C, 400 W; (d) 852 °C, 0 W.

a high-purity N_2 atmosphere (30 mL/min). For isothermal gasification, reaching a temperature of 1000 °C, N_2 was changed to CO_2 (30 mL/min). For overgasifying the CO_2 char, a computer was used to continuously record the sample weight. The conversion of carbon (X)[45−47] was determined as follows:

$$X = \frac{w_0 - w_t}{w_0} \times 100\% \quad (1)$$

where w_0 is the char sample's initial mass and w_t represents the instantaneous char sample mass at any time. The $R_{0.5}$ is calculated in eq 7.

Figure 8a shows the carbon conversion of coal char samples obtained from comparative experiments during isothermal gasification in TGA. As observed in Figure 8a, the carbon conversion of char obtained under condition (c) was higher than those of char obtained under other conditions. The carbon conversion of char obtained under condition (d) was lower than those of char obtained under other conditions. The carbon conversions under conditions (a) and (b) were similar. Figure 8b shows the reactivity index $R_{0.5}$ calculation results based on the data from Figure 8a. The $R_{0.5}$ of char obtained under condition (b) was slightly smaller than that of char obtained under condition (a). This verified that adding the Ni−Cr alloy wire promoted crystalline carbon production in the char, which resulted in a decrease in gasification reactivity to some extent. The $R_{0.5}$ of char obtained under condition (d) was smaller than that of char obtained under condition (b). This was because as the heat treatment temperature increased, the graphitization degree of char increased,[48,49] and the amounts of C−O and C−H in char decreased,[50] resulting in poorer gasification reactivity of char obtained from condition (d) than from condition (b). This indicated that the Ni−Cr wire and higher local temperature in the ECG reduce the gasification reactivity of char to varying degrees.

The $R_{0.5}$ of char obtained under condition (c) is the largest in comparison to those of char obtained under other conditions. This indicated that thermal electrons can effectively improve the gasification reactivity of char in ECG, which is consistent with the XRD test results. These electrons might enhance organic compound cracking and reduction,[32,34,51] hinder the graphitization of coal char during gasification, and finally improve the gasification reactivity of coal char.

This speculation was confirmed by characterizing the chars' chemical structure acquired from the comparative tests via FTIR measurements. The FTIR spectra of char obtained under conditions (a−d) were collected (Figure 9), where the absorbance at approximately 3431 cm^{-1} was associated with the stretching vibration of −OH groups in phenols and other alcohols or aliphatic compounds.[52] Absorbances at approximately 2974 and 2921 cm^{-1} were ascribed to the $-CH_2-$ stretching vibrations of alicyclic and aliphatic hydrocarbons, respectively, and the absorbance at approximately 2851 cm^{-1} was related to the $-CH_3$ stretching vibrations of aliphatic hydrocarbons.[53] Absorbances at approximately 1751 and 1720 cm^{-1} were attributed to the C═O stretching vibrations of aliphatic and aromatic compounds, while the absorbance near 1590 cm^{-1} represented aromatic —C═C— stretching vibrations.[53] The absorbance at approximately 1450 cm^{-1} was allocated to the C−H deformation vibration of alkyl chain structures, and the bands near 1170 and 720 cm^{-1} represented the C−H and ring bending vibrations in aromatics. The absorbance at approximately 1100 cm^{-1} was ascribed to the Si−O−(Si/C) stretching vibrations of silicon compounds within char carbon frame structures.[52]

To analyze the FTIR spectral data more extensively, the hydrogen-enrichment (I_H), aliphatic-structural (I_{AL}), aromatization degree (I_{AR}), and oxygen-enrichment degree (I_{O2}) parameters were calculated from these spectra. The I_H parameter was used to characterize the aliphatic hydrocarbon content and hydrocarbon generation potential, while the I_{AL} parameter assessed the chain length and chain branching degree. The I_{AR} parameter characterized the aliphatic structures on aromatic nuclei and indicated the degree of char thermal evolution, and the I_{O2} parameter was used to assess the number of oxygen-containing functional groups in the char. The specific calculation method for these parameters is as follows:[54]

$$I_H = (A_{V(CH_2)} + A_{V(CH_3)})/A_{V(C=C)} \quad (2)$$

Table 1. Derived Structure Parameters after the Curve Fitting of Diffractograms

samples	L_a (Å)	L_c (Å)	d_{002} (Å)	L_a/L_c	n	crystallinity (%)	f_a
char (a)	0.715	6.840	3.330	0.105	2.054	41.140	0.582
char (b)	0.821	6.808	3.328	0.121	2.045	41.620	0.570
char (c)	0.703	6.729	3.329	0.104	2.022	36.900	0.488
char (d)	0.840	6.856	3.329	0.123	2.060	42.380	0.604

https://doi.org/10.1021/acsomega.1c04135
ACS Omega 2021, 6, 31026−31036

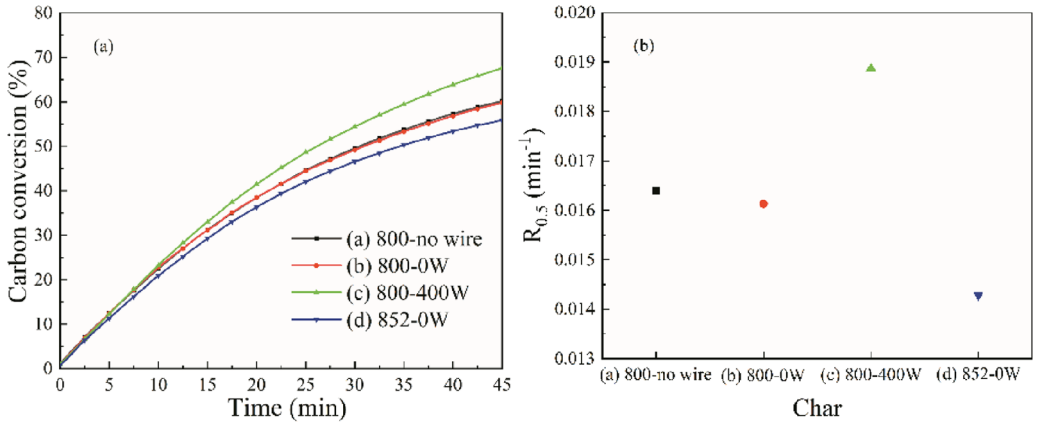

Figure 8. Carbon conversion and reactivity index of char isothermal gasification at 1000 °C determined with TGA: (a) carbon conversion; (b) reactivity index.

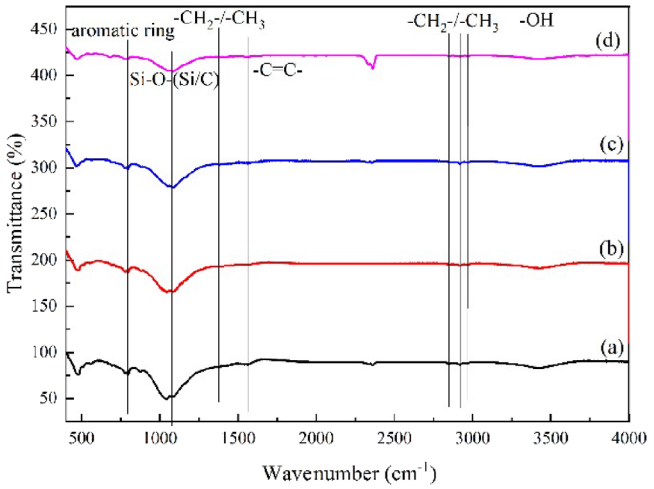

Figure 9. FTIR spectra for the char obtained from the comparative experiment: (a) 800 °C, no wire; (b) 800 °C, 0 W; (c) 800 °C, 400 W; (d) 852 °C, 0 W.

$$I_{AL} = A_{V(CH_2)}/A_{V(CH_3)} \quad (3)$$

$$I_{Ar} = A_{V(CH_2+CH_3)}/A_{V(C=C)} \quad (4)$$

$$I_{O_2} = A_{V(C=O)}/A_{V(C=C)} \quad (5)$$

The calculation results are listed in Table 2. The I_H, I_{AL}, I_{AR}, and I_{O2} parameters of char obtained under condition (b) were lower than those of char produced under condition (a). The Ni−Cr wire promoted the aromatization of the coal char itself, causing it to undergo substantial thermal evolution. Ni in the wire could promote the cracking of macromolecular aliphatic groups in coal char and the precipitation of relatively small molecular aliphatic hydrocarbons;[44] however, the Ni−Cr wire could not prevent the further thermal growth of coal char observed in this study. The I_H, I_{AL}, I_{AR}, and I_{O2} parameters of char obtained under condition (d) were lower than those of char produced under condition (b). The chain length of the aliphatic hydrocarbons in coal char did not significantly change between conditions (b) and (d). However, because of the higher maximal temperature gradients of the coalbeds during ECG, the thermal evolution degree of coal char deepened, and the aromatization reaction intensified, which led to an increase in the proportion of stable aromatic carbons in organic compounds of coal char.

Table 2. Parameter and Indexes of FTIR Spectra

char	a	b	c	d
hydrogen enrichment parameter I_H	2.577	2.291	2.911	2.076
aliphatic structural parameter I_{AL}	2.715	2.640	3.830	2.641
aromatization degree parameter I_{Ar}	1.049	0.862	1.074	0.732
oxygen enrichment degree parameter I_{O2}	13.518	10.639	14.164	8.714

The I_H, I_{AL}, I_{AR}, and I_{O2} parameters of char obtained under condition (c) were higher than those of char produced under other circumstances. This indicates that the degree of aromatization and thermal evolution of coal char obtained under condition (c) is the lowest compared to coal char obtained under other conditions. This is because the ring opening and cracking of aromatic compounds were promoted to a certain extent by thermal electrons,[32,34,51] and further chain aliphatic compounds were created. Organic compound dissociation (e.g., alcohols and carboxylic acids) may form anionic hydrocarbon fragments ($C_xH_y^-$). These compounds were depolymerized from coal with thermal electrons (i.e., $e^-(s) + C_xH_yOH(s)/C_xH_y = C_mH_n^- + ...$) and by the cracking of aromatic compounds.[34,35] Such fragments may then be integrated with coal char via condensation reactions, which give further aliphatic hydrocarbons to the coal char and hinder its deeper thermal evolution and aromatization during ECG.

In addition, by comparison of the I_{O2} of the samples from comparative experiments, it is observed that the char obtained under condition (c) (ECG) also has more oxygen-comprising functional groups than char obtained under other circumstances. This is because CO_2 electroreduction could occur close to the Ni−Cr wire, reaching the reduced CO_2^- anion radicals over the Ni−Cr surface and producing oxalate ions.[51] Oxalate ions may be reduced to give glyoxylate and glycolate anions. Afterward, the coal char may combine with these carboxyl products to increase the number of oxygen-containing functional groups, which would consequently enhance its gasification reactivity,[55] thereby leading to an increase in carbon conversion and combustible gas concentration during ECG.

https://doi.org/10.1021/acsomega.1c04135
ACS Omega 2021, 6, 31026−31036

3. CONCLUSIONS

The reactivity of coal increased with increasing temperature and power during ECG. As these parameters increased, the concentrations of H_2 and CO also increased. However, while the CH_4 concentration increased with power, it only initially increased with increasing temperature and then steadily decreased. The gasification reactivity and concentrations of combustible components produced during gas generation of the ECG process were higher than those of the CCG process. In ECG, by adjusting the power, the efficient gasification of coal can be realized at a relatively low reaction temperature. The application of this method could avoid the problems commonly encountered with conventional catalysts during industrial-scale development, such as extensive equipment corrosion and secondary pollution to the environment.

Thermal electron release is the main reason for the higher effectiveness of ECGs. Thermal electrons could promote ring opening reactions and cracking of aromatic compounds. This electron release could also inhibit aromatization reactions and increase the number of oxygen-containing functional groups in char, which could consequently improve the char gasification reactivity. However, the underlying mechanism still requires further work and understanding.

4. EXPERIMENTAL SECTION

4.1. Sample Preparation and Characterization. Fuxin (FX) coal (Fuxin City, Liaoning Province), a low-grade lignite, was used to prepare the samples under normal laboratory conditions. Samples were ground after drying and sieved to reach an average particle size of approximately 165 μm.

Proximate analysis was performed through thermogravimetric analysis (TGA) conducted using an automatic proximate analyzer (5E-MAG6700, Changsha Kaiyuan Instruments, China). A CHNS/O elemental analyzer (Vario EL III, Elementar, Germany) was used for ultimate analysis. The inorganic chemical composition of the coal was determined using X-ray fluorescence spectrometry (XRF). The test results of these analyses are shown in Table 3.

Table 3. Test Results of Coal Samples[a]

proximate analysis[ad] (mass %)								
moisture		volatile matter			fixed carbon		ash	
3.13		32.77			49.80		14.30	
ultimate analysis[daf] (mass %)								
C		H		O*		N	S	
63.30		5.09		28.82		1.32	1.47	
inorganic chemical composition[d] (mass %)								
SiO_2	SO_3	Al_2O_3	Fe_2O_3	K_2O	CaO	TiO_2	Na_2O	MgO
6.58	3.03	2.51	1.16	0.72	0.30	0.22	0.14	0.13

[a]ad, air-dried basis; d, dry basis; daf, dry ash free basis; *, by difference.

4.2. Reaction System and Operating Procedure. The ECG system (Figure 10) primarily contained a feeding system, reaction system, and analysis system for gas production. Among them, the feeding system mainly includes a gas cylinder and coal feeder that were mainly used to provide coal and gasification agents to the reaction system. The reaction system is a fixed bed reactor with a Ni−Cr wire inside. By inserting a ceramic column within the reactor, the coalbed's height was raised to increase the contact area between the resistance wire and coal. The ceramic support and silica sand were used to fix the bed at the center of the reactor. The analysis system for gas production mainly includes a wash bottle, condensing plant, drying column, gas analyzer, and computer. The wash bottle was used for remove the solid impurities in produced gas. The condensing plant and drying column were used to remove water in produced gas.

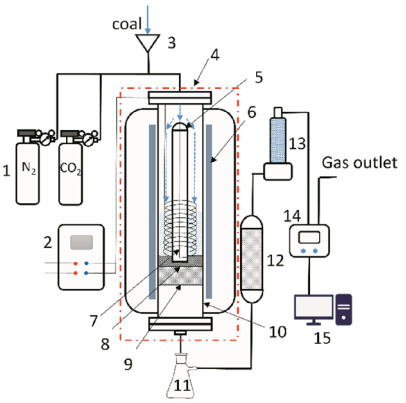

1. CO_2 and argon cylinder, 2. Voltage regulator, 3. Coal inlet, 4. Fixed bed reactor, 5. Ceramic column, 6. External heater, 7. Ni-Cr wire, 8. Silica sand, 9. Ceramic support, 10. Corundum tube, 11. Wash bottle for gases, 12. Gas condensing plant, 13. Drying column, 14. Gas analyzer, 15. Computer

Figure 10. Schematic of the ECG system.

All gasification experiments were performed at atmospheric pressure using this ECG system. Coal samples were introduced into the reactor via the top inlet, after which CO_2 (gasification agent) and N_2 (carrier gas) gases were fed into the reactor at controlled flow rates. Thermocouples were used to measure the temperature distribution of the coalbed.

Both common coal gasification (CCG) and ECG experiments were conducted, where the latter employed an annular Ni−Cr wire surrounding a ceramic column that was mounted in the reactor's center. This wire, while electrified, was used to provide thermal electrons and part of the heat to the coal simultaneously. When the reactor temperature for ECG reached the experimental temperature, N_2 was employed to feed FX coal (6 g) and CO_2 into the reactor through its top inlet. Coal was evenly embedded around the Ni−Cr alloy wire between the outer wall of the ceramic column and the inner wall of the reactor. To achieve a definite reaction temperature, the coalbed was also heated by an external auxiliary furnace. Within the CCG experiment, the structure of the system was similar to that of ECG, except for the lack of an annular Ni−Cr wire mounted in the reactor center, and the coal was heated with only an external auxiliary furnace.

The produced gas passes through the gas washing cylinder, condenser, and dryer in turn and finally enters the gas analyzer.

4.3. Characterization. An online nondispersive infrared (NDIR) gas analyzer (GASBOARD-3100P, China) was used to analyze the compositions of the gas products obtained from the CCG and ECG experiments. The parameters of sensors for the different gases were as follows: CO_2 range, 25%, resolution, 0.01%, and precision, ≤2%; CO range, 50%, resolution, 0.01%, and precision, ≤2%; H_2 range, 25%, resolution, 0.01%, and precision, ≤2%; and CH_4 range, 25%, resolution, 0.01%, and precision, ≤2%. The data were obtained by repeating the measurements three times.

https://doi.org/10.1021/acsomega.1c04135
ACS Omega 2021, 6, 31026−31036

The ECG performance of FX coal was studied via the main combustible gas composition and carbon conversion. The carbon conversion is the percentage of the total molar carbon in the syngas products (excluding trace components such as ethane) to molar carbon in the feed coal, which is calculated using the following equation (eq 6):[3]

$$\eta_c = \frac{(n_{CO} + n_{CH_4} + n_{CO_2out} - n_{CO_2in})}{n_{coal}} \times 100\% \quad (6)$$

where n_{CO}, n_{CH4}, and n_{CO2out} are the moles of CO, CH_4, and CO_2, respectively, in the syngas emitted from the gas outlet of the system. Additionally, n_{CO2in} represents the moles of carbon in the CO_2 gasification agent, and n_{coal} is the moles of carbon in the feed coal. The reactivity index ($R_{0.5}$) can be considered a good indicator of char reactivity during gasification. The $R_{0.5}$ value was determined as the reciprocal of twice the time required for 50% carbon conversion, which is calculated using the following equation (eq 7):[56]

$$R_{0.5} = \frac{0.5}{\tau_{0.5}} \quad (7)$$

where $\tau_{0.5}$ corresponds to the time (min) required for 50% carbon conversion.

The structural change in the char obtained from CCG and ECG experiments was investigated using XRD. To record the XRD patterns of char samples, an X'pert Pro Philips diffractometer was used (Bruker-axs D8 Advance, Germany) with Cu-Kα radiation. A nickel K_β filter was used to eliminate K_β radiation, and the 2θ value ranged from 10 to 85°. Jade 6 software was used to fit the diffractograms in the 2θ regions at approximately 16−33 and 36−53°. Two peaks at approximately 23 and 26° were the (γ) band and (002) plane band, respectively. The peak positions, intensities, widths, and areas were determined.

Structural parameters, such as the average stacking height (L_c) and the average diameter of the layer structure (L_a), were calculated by conventional Scherrer equations[43]

$$L_a = \frac{1.84\lambda}{\beta_a \cos\varphi_a} \quad (8)$$

$$L_c = \frac{1.84\lambda}{\beta_c \cos\varphi_c} \quad (9)$$

where λ is the radiation wavelength; β_a and β_c are the full widths at half-maximum (FWHMs) of the (100) and (002) peaks, respectively; and φ_a and φ_c are the peak positions of the (100) and (002) peaks, respectively. The aromaticity (f_a) is the ratio of aromatic carbon atoms in coal, which was defined as follows:[57]

$$f_a = \frac{A_{002}}{A_{002} + A_r} \quad (10)$$

where A_{002} and A_r are the integrated areas under the 002 peak and γ peak, respectively. The interlayer spacing (d_{002}) was calculated by the Bragg equation[57]

$$d_{002} = \frac{n\lambda}{2\sin\frac{\varphi_c}{2}} \quad (11)$$

where n is the order of reflection, $n = 1$.

The functional groups of char samples obtained from the CCG and ECG experiments were identified by Fourier transform infrared (FTIR) spectroscopy conducted on an FTIR spectrometer (Nicolet Magna760, USA). The spectral range was 400−4000 cm^{-1}, the resolution was 4 cm^{-1}, and the scanning time was 32 s^{-1}.

4.4. Comparative Experiment. In the prior research,[39] it is verified that ECG is indeed superior to CCG. However, compared with CCG, ECG employs a Ni−Cr alloy wire in the coalbed, and nickel and its compounds were shown to influence the release of volatiles during gasification.[44] The temperature distributions of the coalbeds for ECG and CCG were completely different. As shown in Figure 2, thermocouples were arranged at the corresponding positions of the bed to measure the temperature distribution of the coalbed. The coalbed temperature distribution results are shown in Table 4. By electrifying the Ni−Cr wire, the coalbed's temperature close to the Ni−Cr wire became higher than at any other spot of the coalbed.

Table 4. Temperature Distributions in the Coalbed for CCG and ECG Modes

			T_{ECG}
T_{exp} (°C)	P (x, y)[a]	T_{CCG} (°C)	P = 400 W
800	(8.25, 15)	801	808
	(8.25, 0)	802	812
	(8.25, 30)	798	806
	(6, 15)	799	810
	(10.5, 15)	801	804
	$T_{average}$	800.25	808
	$T_{surface}$		852

[a]Coordinates in the ECG coalbed and in the CCG coalbed are represented in Figure 11. The coordinates (8.25, 15) represent the center of the bed, and the unit is mm. T_{ECG} was measured in ECG mode with a power of 400 W, and the unit is °C.

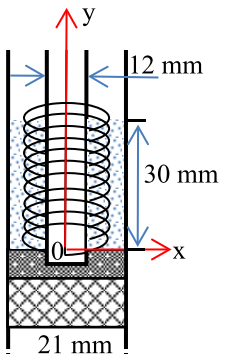

Figure 11. Coordinates of the reactor.

According to Table 4, the temperature deviation between the average coalbed temperature and the coalbed temperature close to the Ni−Cr wire was 44 °C for a heating power of 400 W. Moreover, thermal electrons were released from the Ni−Cr wires during ECG. Thermal electrons were created over the electrified Ni−Cr wires. This observation was found by the anionic time-of-flight mass spectrometry by Yuan et al.[35] Thermal electrons contribute to promoting organic matter decomposition and reformation. Thus, the Ni−Cr wire, thermal electron emission, and coalbed temperature difference may be responsible for the higher carbon conversion and higher combustible gas composition concentration in ECG than in CCG.

https://doi.org/10.1021/acsomega.1c04135
ACS Omega 2021, 6, 31026−31036

To further analyze how the power in the ECG affects the coal gasification process, the effects of three various factors (Ni−Cr wire, thermal electron emission, and coalbed temperature difference) were differentiated through a comparative experiment. The comparative experimental conditions were set to (a) CCG (without the Ni−Cr alloy wire inserted into the coalbed), gasification conditions: T = 800 °C; (b) CCG, with the Ni−Cr alloy wire inserted into the coalbed but not energized, gasification conditions: T = 800 °C; (c) ECG (with the Ni−Cr alloy wire inserted into the coalbed), gasification conditions: T = 800 °C, power = 400 W; and (d) CCG, with the Ni−Cr alloy wire inserted into the coalbed but not energized, gasification conditions: T = 852 °C.

The reaction system and operating procedure are the same as before. When the ceramic support was pushed to the bottom of the reactor (cooling zone), the heating and gasification process simultaneously ceased. Then, the residual char were cooled to room temperature by flushing with N_2. At the end of each experiment, residues were collected for analysis.

For studying the evolution of the char structure in ECG compared to CCG, a char sample with a certain conversion degree must be obtained. However, a different reaction time means different conversion. Because of the limitation of reaction conditions, the collapse of the coal pore structure and the thickening of the ash layer during gasification will affect the contact between the gasification agent and coal char and then inhibit the further reaction of coal char. All of the above reasons will lead to the incomplete reaction of coal under some reaction conditions, that is, there is a maximum carbon conversion. However, under different reaction conditions, the maximum carbon conversion is different. If we want to compare the structural parameters of coal char under different conditions, then the selection of coal char is very important. Under the same conditions, the same carbon conversion means the same extent of reaction; under different conditions, the same carbon conversion cannot represent the same extent of reaction. If coal char with the same carbon conversion is selected, then the extent of the reaction of coal char is different under different conditions. If coal char with the same heating time is selected, then the extent of the reaction of coal char is also different under different conditions. After careful consideration, we decided that it is more reasonable to select coal char with the same extent of reaction under different conditions for comparison.

To compare the char structure evolution during ECG and CCG, a char sample with a certain extent of reaction must be obtained. Since different reaction times induce different levels of conversion, char samples that correspond to the same extent of reaction can be obtained by halting gasification after a certain time under different conditions. To better describe the extent of the reaction, we define the relative carbon conversion as follows:

$$\eta_r = \frac{\eta_c}{\eta_{max}} \times 100\% \quad (12)$$

where η_r is the relative carbon conversion, η_c is the actual carbon conversion, and η_{max} is the maximum carbon conversion under specific conditions. Thus, even under different reaction conditions, the extent of reaction of coal char with the same relative carbon conversion is the same. The char collected was then further characterized.

When the coal was gasified under condition (a), the coal was gasified in CCG mode. When the coal was gasified under condition (c), the coal was gasified in ECG mode. Compared to condition (a), there was a Ni−Cr alloy wire in the coalbed without a current when the coal was gasified under condition (b). By comparing the char obtained under conditions (a) and (b), we can draw a conclusion about how the Ni−Cr alloy wire affects the structure of the char during the ECG process. Table 4 shows that the highest temperature of the bed was 852 °C near the resistance wire under ECG with a power of 400 W. Therefore, compared to condition (b), the temperature of the coalbed was 852 °C when the coal was gasified under condition (d). By comparing the char obtained under conditions (b) and (d), we can draw a conclusion about how changes in the coalbed temperature affect the structure of the char during the ECG process. Similar to condition (d), there is also a Ni−Cr alloy wire in the coalbed, and the maximum temperature of the coalbed was 852 °C when the coal was gasified under condition (c). However, compared to condition (d), the Ni−Cr alloy wire in the coalbed was energized when the coal was gasified under condition (c). By comparing the char obtained under conditions (c) with (d) and other conditions, we can draw a conclusion about how thermal electron emissions affect the structure of char during the ECG process.

AUTHOR INFORMATION

Corresponding Author

Qingbo Yu − *School of Metallurgy, Northeastern University, Shenyang, Liaoning 110819, P.R. China;* orcid.org/0000-0003-0777-1484; Phone: +86-024-83672216; Email: yuqb@smm.neu.edu.cn; Fax: +86-024-83672216

Authors

Fan Yang − *School of Metallurgy, Northeastern University, Shenyang, Liaoning 110819, P.R. China;* orcid.org/0000-0002-0168-4374

Wenjun Duan − *School of Metallurgy, Northeastern University, Shenyang, Liaoning 110819, P.R. China*

Zhenfei Qi − *School of Metallurgy, Northeastern University, Shenyang, Liaoning 110819, P.R. China*

Qin Qin − *School of Metallurgy, Northeastern University, Shenyang, Liaoning 110819, P.R. China*

Complete contact information is available at: https://pubs.acs.org/10.1021/acsomega.1c04135

Notes

The authors declare no competing financial interest.

ACKNOWLEDGMENTS

This research was supported by the Major State Research Development Program of China (2017YFB0603603), the Liaoning Revitalization Talents Program (XLYC1802003), the National Natural Science Foundation of China (51576035), and the Fundamental Research Funds for the Central Universities (N2025006).

REFERENCES

(1) *BP Statistical Review of World Energy*; https://www.bp.com/en/global/corporate/energy-economics/statistical-review-of-world-energy.html (accessed 13 June).

(2) Lobo, L. S.; Carabineiro, S. A. C. Kinetics and mechanism of catalytic carbon gasification. *Fuel* **2016**, *183*, 457−469.

https://doi.org/10.1021/acsomega.1c04135
ACS Omega 2021, 6, 31026−31036

(3) Fan, S.; Yuan, X.; Zhao, L.; Xu, L.-H.; Kang, T.-J.; Kim, H.-T. Experimental and kinetic study of catalytic steam gasification of low rank coal with an environmentally friendly, inexpensive composite K_2CO_3−eggshell derived CaO catalyst. *Fuel* **2016**, *165*, 397−404.
(4) Zhang, F.; Xu, D.; Wang, Y.; Wang, Y.; Gao, Y.; Popa, T.; Fan, M. Catalytic CO_2 gasification of a Powder River Basin coal. *Fuel Process. Technol.* **2015**, *130*, 107−116.
(5) Wang, Y.; Wang, Z.; Huang, J.; Fang, Y. Catalytic Gasification Activity of Na_2CO_3 and Comparison with K_2CO_3 for a High-Aluminum Coal Char. *Energy Fuels* **2015**, *29*, 6988−6998.
(6) Nzihou, A.; Stanmore, B.; Sharrock, P. A review of catalysts for the gasification of biomass char, with some reference to coal. *Energy* **2013**, *58*, 305−317.
(7) Duan, W.; Yu, Q.; Wang, K.; Qin, Q.; Hou, L.; Yao, X.; Wu, T. ASPEN Plus simulation of coal integrated gasification combined blast furnace slag waste heat recovery system. *Energy Convers. Manage.* **2015**, *100*, 30−36.
(8) Irfan, M. F.; Usman, M. R.; Kusakabe, K. Coal gasification in CO_2 atmosphere and its kinetics since 1948: A brief review. *Energy* **2011**, *36*, 12−40.
(9) Liu, Y.; Guan, Y.-J.; Zhang, K. Na_2CO_3 catalyzed CO_2 gasification of coal char and its intermediate complexes. *Res. Chem. Intermed.* **2018**, *44*, 7789−7803.
(10) Tsubouchi, N.; Mochizuki, Y.; Shinohara, Y.; Hanaoka, Y.; Ohtsuka, Y.; Kuramoto, K.; Matsuoka, K. Catalytic effect of ion-exchanged calcium on steam gasification of low-rank coal with a circulating fluidized bed reactor. *Fuel* **2018**, *234*, 406−413.
(11) Zhang, M.-h.; Chen, X.; Xu, H.-l.; Dong, H. Advanced treatment of printing and dyeing wastewater by activated coke and thermal regeneration of spent activated coke. *Desalin. Water Treat.* **2021**, *229*, 421−429.
(12) Xie, Z.; Liu, Z.; Wang, Y.; Yang, Q.; Xu, L.; Ding, W. An Overview of Recent Development in Composite Catalysts from Porous Materials for Various Reactions and Processes. *Int. J. Mol. Sci.* **2010**, *11*, 2152.
(13) Monterroso, R.; Fan, M.; Argyle, M. D.; Varga, K.; Dyar, D.; Tang, J.; Sun, Q.; Towler, B.; Elliot, K. W.; Kammen, D. Characterization of the mechanism of gasification of a powder river basin coal with a composite catalyst for producing desired syngases and liquids. *Appl. Catal., A* **2014**, *475*, 116−126.
(14) Yang, F.; Yu, Q.; Xie, H.; Zuo, Z.; Hou, L.; Qin, Q. Comparative kinetic study of coal gasification with steam and CO2 in molten blast furnace slags. *Korean J. Chem. Eng.* **2018**, *35*, 1626−1635.
(15) Murakami, K.; Sato, M.; Tsubouchi, N.; Ohtsuka, Y.; Sugawara, K. Steam gasification of Indonesian subbituminous coal with calcium carbonate as a catalyst raw material. *Fuel Process. Technol.* **2015**, *129*, 91−97.
(16) Orío, A.; Corella, J.; Narváez, I. Performance of Different Dolomites on Hot Raw Gas Cleaning from Biomass Gasification with Air. *Ind. Eng. Chem. Res.* **1997**, *36*, 3800−3808.
(17) Wicakso, D. R.; Sutijan; Rochmadi; Budiman, A. Catalytic decomposition of tar derived from wood waste pyrolysis using Indonesian low grade iron ore as catalyst. *AIP Conf. Proc.* **2016**, *1737*, No. 060009.
(18) Nguyen, H. N. T.; Berguerand, N.; Thunman, H. Mechanism and Kinetic Modeling of Catalytic Upgrading of a Biomass-Derived Raw Gas: An Application with Ilmenite as Catalyst. *Ind. Eng. Chem. Res.* **2016**, *55*, 5843−5853.
(19) Kuang, J.-p.; Zhou, J.-h.; Zhou, Z.-j.; Liu, J.-z.; Cen, K.-f. Catalytic mechanism of sodium compounds in black liquor during gasification of coal black liquor slurry. *Energy Convers. Manage.* **2008**, *49*, 247−256.
(20) Jiwei, L.; Xianquan, A.; Qianlin, C.; Yan, X.; Yang, C.; Jifang, Z. Disposable Catalysts for Coal Gasification. *Prog. Chem.* **2018**, *30*, 1455−1462.
(21) He, Q.; Yu, J.; Song, X.; Ding, L.; Wei, J.; Yu, G. Utilization of biomass ash for upgrading petroleum coke gasification: Effect of soluble and insoluble components. *Energy* **2020**, *192*, 116642.
(22) Zhang, M.-h.; Chen, X.; Dong, H. A study on multistep thermal decomposition behavior and kinetics of magnesium nitrate hydrate. *Thermochim. Acta* **2021**, *701*, 178951.
(23) Gabor, A. S.; Yimin, L., *Introduction to Surface Chemistry and Catalysis*; Wiley: New York, 1994, p 362−395.
(24) Yuan, L.; Chen, Y.; Song, C.; Ye, T.; Guo, Q.; Zhu, Q.; Torimoto, Y.; Li, Q. Electrochemical catalytic reforming of oxygenated-organic compounds: a highly efficient method for production of hydrogen from bio-oil. *Chem. Commun.* **2008**, *41*, 5215−5217.
(25) Li, Q. X.; Hayashi, K.; Nishioka, M.; Kashiwagi, H.; Hirano, M.; Torimoto, Y.; Hosono, H.; Sadakata, M. Absolute emission current density of O− from $12CaO{\cdot}7Al_2O_3$ crystal. *Appl. Phys. Lett.* **2002**, *80*, 4259−4261.
(26) Li, Q.; Hosono, H.; Hirano, M.; Hayashi, K.; Nishioka, M.; Kashiwagi, H.; Torimoto, Y.; Sadakata, M. High-intensity atomic oxygen radical anion emission mechanism from $12CaO{\cdot}7Al_2O_3$ crystal surface. *Surf. Sci.* **2003**, *527*, 100−112.
(27) Li, J.; Huang, F.; Wang, L.; Wang, Z.; Yu, S.; Torimoto, Y.; Sadakata, M.; Li, Q. Mechanistic Features for Hydroxyl Anion Emission from the Modified $12CaO{\cdot}7Al_2O_3$ Surface. *J. Phys. Chem. B* **2005**, *109*, 14599−14603.
(28) Li, J.; Huang, F.; Wang, L.; Yu, S. Q.; Torimoto, Y.; Sadakata, M.; Li, Q. X. High Density Hydroxyl Anions in a Microporous Crystal: $[Ca_{24}Al_{28}O_{64}]^{4+}{\cdot}4(OH^-)$. *Chem. Mater.* **2005**, *17*, 2771−2774.
(29) Huang, F.; Li, J.; Xian, H.; Tu, J.; Sun, J. Q.; Yu, S. Q.; Li, Q. X.; Torimoto, Y.; Sadakata, M. Substitution of H^- for O^- and H^- emissions of $12CaO{\cdot}7Al_2O_3$. *Appl. Phys. Lett.* **2005**, *86*, 114101.
(30) Huang, F.; Li, J.; Wang, L.; Dong, T.; Tu, J.; Torimoto, Y.; Sadakata, M.; Li, Q. Features and Mechanism of H^- Anion Emission from $12CaO{\cdot}7Al_2O_3$ Surface. *J. Phys. Chem. B* **2005**, *109*, 12032−12037.
(31) Song, C.; Sun, J.; Qiu, S.; Yuan, L.; Tu, J.; Torimoto, Y.; Sadakata, M.; Li, Q. Atomic Fluorine Anion Storage Emission Material C12A7-$F^-$and Etching of Si and SiO_2 by Atomic Fluorine Anions. *Chem. Mater.* **2008**, *20*, 3473−3479.
(32) Chen, Y.; Yuan, L.; Ye, T.; Qiu, S.; Zhu, X.; Torimoto, Y.; Yamamoto, M.; Li, Q. Effects of current upon hydrogen production from electrochemical catalytic reforming of acetic acid. *Int. J. Hydrogen Energy* **2009**, *34*, 1760−1770.
(33) Backhaus-Ricoult, M. SOFC−A playground for solid state chemistry. *Solid State Sci.* **2008**, *10*, 670−688.
(34) Ye, T.; Yuan, L.; Chen, Y.; Kan, T.; Tu, J.; Zhu, X.; Torimoto, Y.; Yamamoto, M.; Li, Q. High Efficient Production of Hydrogen from Bio-oil Using Low-temperature Electrochemical Catalytic Reforming Approach Over NiCuZn−Al_2O_3 Catalyst. *Catal. Lett.* **2009**, *127*, 323−333.
(35) Yuan, L.; Ye, T.; Gong, F.; Guo, Q.; Torimoto, Y.; Yamamoto, M.; Li, Q. Hydrogen Production from the Current-Enhanced Reforming and Decomposition of Ethanol. *Energy Fuels* **2009**, *23*, 3103−3112.
(36) Li, X.-l.; Ning, S.; Yuan, L.-x.; Li, Q.-x. Hydrogen Production From Crude Bio-oil and Biomass Char by Electrochemical Catalytic Reforming. *Chin. J. Chem. Phys.* **2011**, *24*, 477−483.
(37) Kan, T.; Xiong, J.; Li, X.; Ye, T.; Yuan, L.; Torimoto, Y.; Yamamoto, M.; Li, Q. High efficient production of hydrogen from crude bio-oil via an integrative process between gasification and current-enhanced catalytic steam reforming. *Int. J. Hydrogen Energy* **2010**, *35*, 518−532.
(38) Tao, J.; Lu, Q.; Dong, C.; Du, X.; Dahlquist, E. Effects of electric current upon catalytic steam reforming of biomass gasification tar model compounds to syngas. *Energy Convers. Manage.* **2015**, *100*, 56−63.
(39) Yang, F.; Yu, Q.; Duan, W.; Qi, Z.; Qin, Q. Electrochemical catalytic coal gasification: A novel method. *Catal. Commun.* **2021**, *150*, 106261.
(40) Xie, Y.; Yang, H.; Zeng, K.; Zhu, Y.; Hu, J.; Mao, Q.; Liu, Q.; Chen, H. Study on CO_2 gasification of biochar in molten salts: Reactivity and structure evolution. *Fuel* **2019**, *254*, 115614.

https://doi.org/10.1021/acsomega.1c04135
ACS Omega 2021, 6, 31026−31036

(41) Kashiwaya, Y.; Ishii, K. Kinetic Analysis of Coke Gasification Based on Non-crystal/Crystal Ratio of Carbon. *ISIJ Int.* **1991**, *31*, 440−448.
(42) Ludwig Schoening, F. R. X-ray structure of some South African coals before and after heat treatment at 500 and 1000° C. *Fuel* **1983**, *62*, 1315−1320.
(43) Zhang, Y.; Kang, X.; Tan, J.; Frost, R. L. Influence of Calcination and Acidification on Structural Characterization of Anyang Anthracites. *Energy Fuels* **2013**, *27*, 7191−7197.
(44) Zhong, M.; Zhao, Y.; Zhai, J.-R.; Jin, L.-J.; Hu, H.-Q.; Bai, Z.-Q.; Li, W. Effects of nickel additives with different anions on the structure and pyrolysis behavior of Hefeng coal. *Fuel Process. Technol.* **2019**, *193*, 273−281.
(45) Zuo, Z.; Luo, S.; Liu, S.; Zhang, J.; Yu, Q.; Bi, X. Thermokinetics of mass-loss behavior on direct reduction of copper slag by waste plastic char. *Chem. Eng. J.* **2021**, *405*, 126671.
(46) Zuo, Z.; Luo, S.; Zhang, J.; Yu, Q.; Guo, J.; Bi, X.; Zhou, E. C and CO Reduction Proportional Fraction with Copper Slag by a Phase Equilibrium Calculation Model (PECM). *Energy Fuels* **2020**, *34*, 698−708.
(47) Zuo, Z.; Yu, Q.; Luo, S.; Zhang, J.; Zhou, E. Effects of CaO on Two-Step Reduction Characteristics of Copper Slag Using Biochar as Reducer: Thermodynamic and Kinetics. *Energy Fuels* **2020**, *34*, 491−500.
(48) Fermoso, J.; Gil, M. V.; Borrego, A. G.; Pevida, C.; Pis, J. J.; Rubiera, F. Effect of the Pressure and Temperature of Devolatilization on the Morphology and Steam Gasification Reactivity of Coal Chars. *Energy Fuels* **2010**, *24*, 5586−5595.
(49) Wang, Q.; Zhang, R.; Luo, Z.; Fang, M.; Cen, K. Effects of Pyrolysis Atmosphere and Temperature on Coal Char Characteristics and Gasification Reactivity. *Energy Technol.* **2016**, *4*, 543−550.
(50) Yu, J.; Guo, Q.; Ding, L.; Gong, Y.; Yu, G. Studying effects of solid structure evolution on gasification reactivity of coal chars by in-situ Raman spectroscopy. *Fuel* **2020**, *270*, 117603.
(51) Shoichiro, I.; Takehiko, T.; Kaname, I. Selective Formation of Formic Acid, Oxalic Acid, and Carbon Monoxide by Electrochemical Reduction of Carbon Dioxide. *Bull. Chem. Soc. Jpn.* **1987**, *60*, 2517−2522.
(52) He, Q.; Huang, Y.; Ding, L.; Guo, Q.; Gong, Y.; Yu, G. Effect of Partial Rapid Pyrolysis on Bituminous Properties: From Structure to Reactivity. *Energy Fuels* **2020**, *34*, 5476−5484.
(53) Li, G.-S.; Fan, X.; You, C.-Y.; Zhao, Y.-P.; Wang, R.-Y.; Wei, X.-Y.; Ma, F.-Y.; Lu, X.; Mo, W.-L.; Li, X. Molecular characteristics of the soluble components from three low-rank coals based on the analyses using GC/MS and GC/Q-TOF MS. *Fuel* **2019**, *254*, 115602.
(54) Lin, R.; Ritz, G. P. Reflectance FT-IR Microspectroscopy of Fossil Algae Contained in Organic-Rich Shales. *Appl. Spectrosc.* **1993**, *47*, 265−271.
(55) Li, T.; Zhang, L.; Dong, L.; Qiu, P.; Wang, S.; Jiang, S.; Li, C.-Z. Changes in char structure during the low-temperature pyrolysis in N_2 and subsequent gasification in air of Loy Yang brown coal char. *Fuel* **2018**, *212*, 187−192.
(56) Duan, W.; Yu, Q.; Liu, J.; Hou, L.; Xie, H.; Wang, K.; Qin, Q. Characterizations of the hot blast furnace slag on coal gasification reaction. *Appl. Therm. Eng.* **2016**, *98*, 936−943.
(57) Lu, L.; Sahajwalla, V.; Kong, C.; Harris, D. Quantitative X-ray diffraction analysis and its application to various coals. *Carbon* **2001**, *39*, 1821−1833.

https://doi.org/10.1021/acsomega.1c04135
ACS Omega 2021, 6, 31026−31036